Lymphotoxin β receptor signaling promotes tertiary lymphoid organogenesis in the aorta adventitia of aged *ApoE*$^{-/-}$ mice

Rolf Gräbner,[1] Katharina Lötzer,[1] Sandra Döpping,[1] Markus Hildner,[1] Dörte Radke,[1,3] Michael Beer,[1] Rainer Spanbroek,[1] Beatrix Lippert,[1] Catherine A. Reardon,[4] Godfrey S. Getz,[4] Yang-Xin Fu,[4] Thomas Hehlgans,[5] Reina E. Mebius,[6] Michael van der Wall,[2] Dagmar Kruspe,[7] Christoph Englert,[7] Agnes Lovas,[8] Desheng Hu,[8] Gwendalyn J. Randolph,[9] Falk Weih,[8] and Andreas J.R. Habenicht[1]

[1]Institute for Vascular Medicine, [2]Animal Research Institute, Friedrich Schiller University of Jena, 07743 Jena, Germany
[3]Leibniz-Institute for Natural Product Research and Infection Biology, Hans-Knoell-Institute, 07745 Jena, Germany
[4]Department of Pathology, University of Chicago, Chicago, IL 60637
[5]Institute of Immunology, University of Regensburg, 93053 Regensburg, Germany
[6]Department of Molecular Cell Biology and Immunology, Vrje Universiteit Medical Center, 1007 MB Amsterdam, Netherlands
[7]Research Group Molecular Genetics, [8]Research Group Immunology, Leibniz-Institute for Age Research, Fritz-Lipmann-Institute, 07745 Jena, Germany
[9]Department of Gene and Cell Medicine, Mount Sinai School of Medicine, New York, NY 10029

Atherosclerosis involves a macrophage-rich inflammation in the aortic intima. It is increasingly recognized that this intimal inflammation is paralleled over time by a distinct inflammatory reaction in adjacent adventitia. Though cross talk between the coordinated inflammatory foci in the intima and the adventitia seems implicit, the mechanism(s) underlying their communication is unclear. Here, using detailed imaging analysis, microarray analyses, laser-capture microdissection, adoptive lymphocyte transfers, and functional blocking studies, we undertook to identify this mechanism. We show that in aged *apoE*$^{-/-}$ mice, medial smooth muscle cells (SMCs) beneath intimal plaques in abdominal aortae become activated through lymphotoxin β receptor (LTβR) to express the lymphorganogenic chemokines CXCL13 and CCL21. These signals in turn trigger the development of elaborate bona fide adventitial aortic tertiary lymphoid organs (ATLOs) containing functional conduit meshworks, germinal centers within B cell follicles, clusters of plasma cells, high endothelial venules (HEVs) in T cell areas, and a high proportion of T regulatory cells. Treatment of *apoE*$^{-/-}$ mice with LTβR-Ig to interrupt LTβR signaling in SMCs strongly reduced HEV abundance, CXCL13, and CCL21 expression, and disrupted the structure and maintenance of ATLOs. Thus, the LTβR pathway has a major role in shaping the immunological characteristics and overall integrity of the arterial wall.

CORRESPONDENCE
Andreas J.R. Habenicht:
andreas.habenicht@mti.uni-jena.de

Abbreviations used: α-LTβR, agonistic LTβR antibody; AAA, abdominal aorta aneurysm; ATLO, aorta tertiary lymphoid organ; DN, double-negative; FDC, follicular DC; GC, germinal center; GO, gene ontology; HEV, high endothelial venule; LCM, laser-capture microdissection; LTβ, lymphotoxin β chain; LTβR, LTβ receptor; MAdCAM-1, mucosal addressin cell adhesion molecule 1; PNA, peanut agglutinin; PNAd, peripheral LN addressin; SLO, secondary lymphoid organ; SMA, smooth muscle actin; TLO, tertiary lymphoid organ; TNFRSF1A, tumor necrosis factor receptor superfamily, member 1A.

Most studies of atherosclerosis to date have focused on intima lesions, which are composed of lipid-laden macrophage/foam cells, T cells, and smooth muscle cells (SMCs). These lesion-forming cells elicit persistent inflammation and ultimately trigger adaptive immune responses toward arterial wall–derived autoantigens, such as heat shock proteins or oxidized LDL. However, how and where atherosclerosis inflammation is translated into adaptive immune responses, including T and B cell autoimmunity, remains to be fully understood (1–6). It is unlikely that atherosclerotic intimal lesions carry out critical steps of adaptive immune responses themselves. Although such reactions may occur in secondary lymphoid organs (SLOs), infiltrates of leukocytes in the adventitia of coronary arteries in patients afflicted with atherosclerosis were noted decades ago (7), and adventitial B cell follicle-like aggregates in

The Rockefeller University Press $30.00
J. Exp. Med. Vol. 206 No. 1 233-248
www.jem.org/cgi/doi/10.1084/jem.20080752

The Journal of Experimental Medicine

human aortae were recently described (8). We and others reported that the adventitia of *apolipoprotein-deficient* (*apoE*$^{-/-}$) mice contained T/B cell aggregates (9–11). Although these data supported the concept that arterial wall inflammation spreads from the intima to the adventitia, the impact of adventitial immunity on arterial wall biology remains puzzling and unresolved. Moreover, the mechanism of how the inflammation spreads between the intima and the adventitia is unknown. The cellular composition of the two inflammatory foci is distinct, and there is no histological evidence that inflammatory cells readily traverse the medial SMC compartment to mediate steady and ongoing communication between the intima and adventitia. Indeed, passage of lymphocytes and phagocytes through the medial compartment of great arteries is typically minimal (12), rendering the media itself some of the properties of immunoprivileged tissues.

Here, we have set out to characterize the mechanistic basis of communication between the two compartments, as we have reasoned that meeting the long-term goal of understanding whether the adventitial inflammation has either a beneficial or pathological role in atherosclerosis may require experimental manipulation of the inflammatory response in the adventitia itself. We now report that medial SMCs underlying intimal plaques become activated, and through a lymphotoxin β receptor (LTβR)-dependent signaling pathway, are induced to express CXCL13/CCL21, which in turn drives recruitment of T/B cell aggregates. These aggregates are precursors of fully structured aorta tertiary lymphoid organs (ATLOs) that contain large numbers of regulatory T cells (T reg cells), germinal centers (GCs), high endothelial venules (HEVs), and LN-like conduits that connect ATLOs to the medial SMC compartment and likely sustain and amplify the adventitial response. These data reveal how the intima and adventitia communicate to develop a coordinated reaction, even in an anatomical region where inflammatory cell traffic between the two compartments is limited.

RESULTS

ATLO neogenesis occurs in old *apoE*$^{-/-}$ mice and is confined to lesion-burdened abdominal aorta

We searched for ATLOs in 6–130-wk-old mice ($n = 30$) using a three-stage classification scheme (Fig. S1, available at http://www.jem.org/cgi/content/full/jem.20080752/DC1). ATLO neogenesis was initiated at >32 wk and occurred in ∼75% of mice afflicted with abdominal aorta atherosclerosis at 78 wk. We compared ATLO incidence in the innominate artery with the incidence in the abdominal aorta at 78 wk. Most (8/11) *apoE*$^{-/-}$ mice developed ATLO stage II/III in the abdominal aorta, whereas only 1/11 mice showed a stage I ATLO in the innominate artery (Fig. 1 a). We never observed ATLO formation in aorta segments that were not affected by lesions. Moreover, lesion sizes in the abdominal aorta correlated with ATLO sizes (Fig. 1 b).

Characterization of ATLO cellularity and structure

ATLOs were crescent-shaped and contacted the external lamina, wrapping around portions of or the entire aorta. Diameters of some ATLOs exceeded those of the media and the associated lesions (Fig. 2 a, top left). They showed B cell follicles (B220$^+$; Fig. 2 a, top right) containing ectopic GCs that were equipped with follicular DC (FDC) networks (CD35$^+$; Fig. 2 a, middle left), and separate T cell (CD3ε$^+$) and plasma cell (CD138$^+$) areas (Fig. 2 a, middle right). GCs in B cell follicles showed signs of activation as indicated by proliferating (Ki67$^+$) centrocytes (peanut agglutinin–positive [PNA$^+$]) in GC B cell areas (Fig. 2 a, bottom left) surrounded by follicular mantle (IgD$^+$) B cells (Fig. 2 a, bottom right) (13, 14). Numerous Foxp3$^+$ regulatory T cells (T reg cells) were observed in ATLO T cell areas (Fig. 2 b, left), similar to T areas of the adjacent paraaortic LN (Fig. 2 b, right). ATLOs were supplied with multiple HEVs (peripheral LN addressin positive [PNAd$^+$]; Fig. 2 c, top left), blood vessels (MECA-32$^+$; Fig. 2 c, top right), and lymph vessels (Lyve1$^+$; Fig. 2 c, top right), indicating extensive neoangiogenesis. Similar to autoimmune thyroiditis (15), ATLO-associated lymph vessels had distended lumina caused by large numbers of intraluminal cells (Fig. 2 c, bottom left, open triangles), whereas lymph vessels adjacent to ATLOs did not (Fig. 2 c, bottom right). Unlike paraaortic LNs (Fig. S2, available at http://www.jem.org/cgi/content/full/jem.20080752/DC1), ATLOs contacted the external lamina and lacked capsules including rims of peripheral Lyve1$^+$ cells.

Aorta leukocyte lineage composition changes with age and shows marked differences in thoracic versus abdominal aorta

We previously reported that the formation of T/B cell aggregates follows adventitial T cell infiltration, which parallels intima lesion formation (10). Flow cytometry was used to quantify the aorta leukocyte composition of young and aged wild-type and *apoE*$^{-/-}$ mice. Aorta digests from young (20 wk) and aged (78 wk) wild-type and young *apoE*$^{-/-}$ mice (20 wk) contained few CD45$^+$ leukocytes, corroborating previous morphometric analyses in ≤52 wk *apoE*$^{-/-}$ mice (10) (unpublished data). In contrast, aorta digests of aged *apoE*$^{-/-}$ mice yielded markedly increased numbers of CD45$^+$, CD3$^+$,

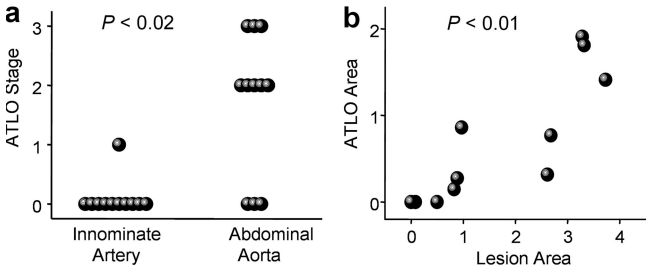

Figure 1. Incidence of ATLOs in different aorta segments and association of ATLOs and plaques. (a) Preferential occurrence of ATLOs in the abdominal aorta; innominate arteries and abdominal aortae were examined for ATLO stages in aged *apoE*$^{-/-}$ mice. chi-Square (χ^2) test, $P < 0.02$. (b) ATLO sizes correlate with plaque sizes; morphometry was performed by determination of plaque size/media size or ATLO size/media size ($n = 11$ mice). Pearson correlation coefficient: 0.783. $P < 0.01$.

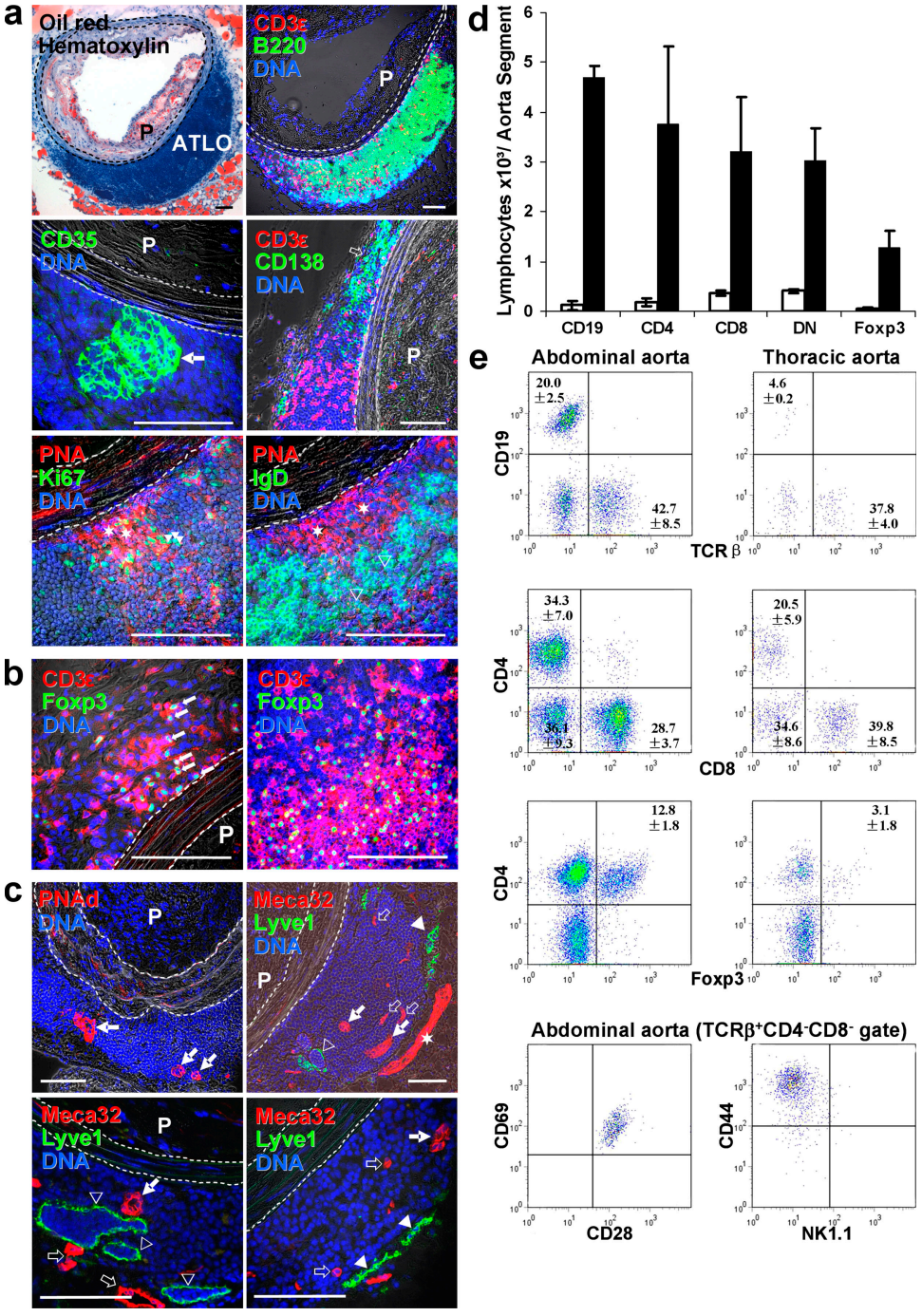

Figure 2. ATLO cellularity and structure and quantification of leukocyte subsets in abdominal and thoracic aorta segments. (a) ATLO position relative to media (dashed lines) and plaque (P) of aged *apoE*$^{-/-}$ mouse (Oil Red O/hematoxylin); B cell follicle (B220); and T cell area (CD3ε). FDCs in GC (CD35, filled arrow), plasma cells (CD138, open arrow), and DAPI (DNA); GCs contain Ki67^{+} (triangles) cells in PNA^{+} areas (asterisks) and follicular mantle B cells (IgD^{+}; open triangles). (b) Foxp3^{+} T reg cells in ATLO T cell area (left, arrows) and in T cell area of paraaortic LN (right). (c) HEVs (PNAd; top left, filled arrows), blood vessels (MECA-32; top and bottom right; filled arrows indicate HEVs, open arrows indicate blood vessels), ATLO lymph vessel (Lyve1; top right and bottom left, open triangles), and normal lymph vessels (top right, filled triangle); asterisk indicates vena cava. Bars: 100 µm. (d) Absolute numbers of lymphocyte subsets per aorta segment (open columns, thoracic aorta; shaded columns, abdominal aorta). CD19, $P < 0.0005$; CD4, $P < 0.05$; CD8, n.s.; DN, $P < 0.005$; Foxp3, $P < 0.02$; one-sided unpaired Student's *t* test. (e) Flow cytometric analysis of aortae from old *apoE*$^{-/-}$ mice. Aortae were separated into similarly sized abdominal and thoracic segments, and single-cell suspensions were analyzed for expression of CD19/TCRβ (top two plots, lymphocyte gate within the CD45^{+} population), as well as CD4/CD8 and CD4/Foxp3 (middle four plots, TCRβ^{+} gate within CD45^{+} lymphocytes). TCRβ^{+} CD4^{-}CD8^{-} DN T cells from the abdominal aorta were further characterized for CD69/CD28 and CD44/NK1.1 expression (bottom two plots, TCRβ^{+}CD4^{-}CD8^{-} gate). DN T cells were also CD25^{+}Foxp3^{-} (not depicted). Numbers in quadrants represent percentages of positive cells (mean values ± SD; *n* = 7–12 mice).

and CD19$^+$ leukocytes (unpublished data). We next quantified lymphocyte subsets in thoracic versus abdominal aorta segments of aged *apoE*$^{-/-}$ mice. Absolute numbers of each lymphocyte subset, including both T reg cell subsets (Fig. 2 d), was much higher in the abdominal compared with thoracic aorta segments, thus substantiating the immunohistochemical characterization of ATLO cellularity (Fig. 1, a–c). The number of B cells (CD19$^+$) in thoracic aorta (Fig. 2 e, top right) was low, whereas a large percentage of abdominal aorta leukocytes were B cells (CD19$^+$; Fig. 2 e, top left). Similar to paraaortic LNs, the expanded ATLO T cell compartment contained considerable numbers of CD3$^+$/CD4$^+$/CD25$^+$/Foxp3$^+$ T reg cells (Fig. 2 e) (16). Moreover, increased numbers of TCR$^+$/CD3$^+$/CD4$^-$/CD8$^-$ double-negative (DN) T cells were found in abdominal aorta segments compared with the thoracic aorta (Fig. 2 e) (17, 18). Interestingly, aortic DN T cells had a marker profile (TCRβ$^+$/CD3$^+$/CD4$^-$/CD8$^-$/NK1.1$^-$/CD44$^+$/CD25$^+$/CD69$^+$/ CD28$^+$/Foxp3$^-$; Fig. 2 e, bottom) that resembled T reg cells, which were recently shown to suppress alloimmune responses (18).

Overall, these data indicate that (a) ATLO neogenesis is preferentially located in the abdominal aorta; (b) ATLO neogenesis exclusively occurs in aorta segments afflicted with severe atherosclerosis; (c) ATLO size correlates with plaque size; (d) ATLOs develop in aged *apoE*$^{-/-}$, but not aged wild-type, mice; (e) ATLO neogenesis is characterized by marked B cell accumulation at various stages of maturation and accompanied by substantial absolute increases in several lymphocyte subsets; and (f) a considerable percentage of ATLO T cells are CD3$^+$/CD4$^+$/CD25$^+$/Foxp3$^+$ or TCRβ$^+$/CD3$^+$/CD4$^-$/CD8$^-$/Foxp3$^-$ T reg cells.

ATLOs promote lymphocyte recruitment and recirculation into the arterial wall

To examine the ability of ATLOs to actively promote lymphocyte recruitment and/or recirculation into the arterial wall, we performed adoptive transfer experiments in aged *apoE*$^{-/-}$ mice using naive 12-wk-old wild-type splenocytes labeled with CFSE (19). At 3 h after transfer, CFSE$^+$ cells were observed in ATLOs, although more cells were present in regional LNs and spleen (unpublished data). However, at 18 h (when >90% of the transferred cells had left the circulation), ATLOs contained considerable numbers of lymphocytes (Fig. 3 a), whereas none or only few were observed in adjacent adventitia, retroperitoneal paraaortic adipose tissue, media, or atherosclerotic plaques (Fig. 3 a and not depicted). CFSE$^+$ cells were readily detected throughout all ATLO compartments, although most cells localized to T cell areas (Fig. 3 b, left 4 images, arrows). Colocalization studies of CFSE with CD3 and B220 indicated a preference of recruited cells for T cells (Fig. 3 b, Merge). Many CFSE$^+$ cells colocalized with PNAd$^+$/Meca32$^+$ HEVs (Fig. 3 b; right open arrows), but none with PNAd$^-$/Meca32$^+$ blood vessels (Fig. 3 b, right asterisks; Fig. S3 and Video 1, available at http://www.jem.org/cgi/content/full/jem.20080752/DC1). Thus, ATLOs promote high rates of T cell recruitment into the arterial wall on an ongoing basis from the bloodstream, most likely through HEVs.

Lesion and ATLO genes signify separable immune responses

Because lesion gene expression should become detectable at 32 wk (10) and ATLO gene expression may follow at 78 wk (see above), aorta gene expression microarrays from 6-, 32-, and 78-wk-old mice were prepared following MIAME guidelines (www.ncbi.nlm.nih.gov/geo/info/MIAME.html; data were deposited in National Center for Biotechnology Information's gene expression omnibus, GEO accession no. GSE10000). Differentially up-regulated genes in *apoE*$^{-/-}$ mouse aortae were identified (Table S1, available at http://www.jem.org/cgi/content/full/jem.20080752/DC1). A fuzzy c-means cluster algorithm defined two clusters differing in their onset of gene up-regulation (Fig. S4): an early (32 wk) atherosclerosis cluster and a late (78 wk) *ATLO* cluster (Fig. 4 a). Genes up-regulated at 32 wk largely mirrored the influx of monocytes into lesions (Fig. 4 a and Table S1), whereas genes up-regulated at 78 wk mirrored TLO neogenesis and B cell immunity (Fig. 4 a and Table S1). Gene ontology (GO) terms cytokine activity, cytokine binding, and immunoglobulin binding in the atherosclerosis cluster and

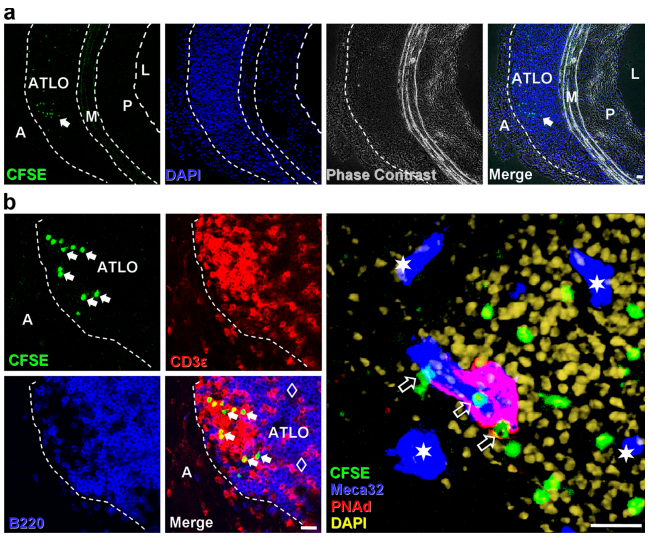

Figure 3. ATLOs promote lymphocyte recruitment and recirculation into the arterial wall. CFSE labeling and i.v. application of splenocytes was performed as described in Materials and methods. 18 h later, aorta was prepared and consecutive sections were examined. (a) Overview of abdominal aorta segment with adjacent intima lesion and ATLO at 18 h reveals selective presence of CFSE$^+$ splenocytes in ATLO, but none in adjacent adventitia, media, or plaque (filled arrow). Unspecific autofluorescence was subtracted from the specific CFSE-related fluorescence as described in Materials and methods. L, lumen; A, adventitia; M, media; P, plaque. (b) CFSE$^+$ splenocytes preferentially accumulate in ATLO T cell area (left images, filled arrows) when compared with B cell follicles (open diamonds); CFSE$^+$ cells are associated with HEVs (MECA-32$^+$PNAd$^+$ structure, open arrows), but not with blood vessel lumina (MECA-32$^+$PNAd$^-$ structures, asterisks; Video 1, available at http://www.jem.org/cgi/content/full/jem.20080752/DC1). Bars, 20 µm.

cytokine activity, chemokine receptor activity, and antigen binding in the ATLO cluster exemplified the differentially expressed genes in plaques versus ATLOs (Fig. 4 a). The ATLO cluster contained the following genes not previously associated with atherosclerosis: genes regulating B cell recruitment/maturation, GC formation, and autoimmunity, including *Cxcl13*, *Ccl21*, and *Ltb* (Fig. 4 a). Thus, genes of the atherosclerosis and ATLO clusters selectively emerged in the diseased aorta in a statistically significant stepwise fashion. Selected transcripts were confirmed by quantitative RT-PCR (Fig. S5).

Laser capture microdissection (LCM) microarrays reveal differential gene expression in ATLOs versus plaques

The stark differences in the overall gene expression patterns between *apoE*$^{-/-}$ aortae at 32w versus 78w likely reflected the emergence, and dominance, of genes expressed in the ATLOs. To verify this possibility, we selected areas of the abdominal aorta with advanced plaques and separated plaques and corresponding ATLOs by LCM. Adventitia of aorta segments that were not associated with atherosclerosis and adventitia of wild-type mice served as controls. Wild-type adventitia (10) microarrays showed gene signatures that resembled plaque-free adventitia of *apoE*$^{-/-}$ mice (Fig. 4 b; Supplementary Table S2). Adventitia in aorta segments with associated ATLOs contained numerous genes known to regulate TLO formation including *Cxcl13*, *Ccl21*, and *Ltb* (Fig. 4 b). In contrast, plaques showed prototypic atherosclerosis genes (Fig. 4 b). Genes induced in the adventitia during ATLO neogenesis but absent from plaques are *Glycam1* (exclusively expressed by HEV endothelial cells involved in T cell recruitment) and *Ccl21* (a T cell chemokine). In situ hybridization combined with immunohistochemical analyses of parallel thin sections (data not shown) demonstrated *Glycam1* mRNA signals in ATLO HEVs (Fig. 4 c) but none in media or plaques. Similarly, we observed *Ccl21* mRNA signals in HEVs and adventitial lymph vessels (Fig. 4 c). When taken together, these data establish topographical large-scale transcriptome maps for ATLOs versus adjacent lesions proper and reveal a marked dichotomy in adventitial and lesion immune response-regulating genes in diseased aortae.

LN-like conduits connect media SMCs to ATLOs and transport low molecular weight molecules

Although gene expression patterns were distinct between the adventitia and plaques, the dependence of ATLOs on intimal lesion development suggested that the compartments communicate. Antigen reaches LNs via migration of antigen-loaded DCs or via directed diffusion through a specialized conduit system that connects afferent lymph vessels and HEVs (20–22). Conduits have not previously been studied in TLOs (23). Owing to their size, conduits cannot transport cells but form a reticular meshwork of fibers consisting of a rodlike core of collagen I wrapped by extracellular matrix sheaths enfolded by podoplanin-expressing fibroblastic reticular cells. Staining with ER-TR7 (unknown antigen) and 8.1.1 (podoplanin/gp38) revealed a reticular meshwork of cordlike structures (Fig. 5 a) in ATLOs. ER-TR7/8.1.1/DAPI staining confirmed colocalization of 8.1.1 with fibroblastic reticular cells adjacent to ER-TR7^{+} cords (Fig. 5 a, top). ATLO conduits were further identified by their small diameter (conduits, ~2 μm; capillaries, ~4 μm), the absence of MECA-32 staining, and the presence of a collagen I core (unpublished data). Because conduits near the adventitia-media border appeared denser, we examined whether they extend into the media. 3D reconstruction of high resolution laser scanning microscopy of stage III ATLOs revealed that ATLO conduits extended into the media gaining access to HEVs of ATLO T areas and other ATLO compartments (Fig. 5 a, bottom left; Fig. S6; Fig. S7 and Video 2; and Fig. S8 and Video 3, available at http://www.jem.org/cgi/content/full/jem.20080752/DC1). To explore the functionality of ATLO conduits in vivo we used fluorescent dextran particles. After i.v. application, 10 kD dextran, but not 500 kD dextran, particles were taken up by ATLO conduits similar to LN conduits (Fig. 5 b and not depicted). Thus, ATLO conduits resemble LN conduits in size, marker expression, and transport function and establish newly formed structures connecting the adventitia to the media.

Media SMCs sandwiched between lesions and ATLOs are activated and express CXCL13 and CCL21

Because embryonic SLO formation requires CXCL13 and CCL21 chemokines (24–26), and ectopic expression of CXCL13 is sufficient to induce TLOs (27), we searched for CXCL13/CCL21 in ATLOs. Surprisingly, media segments sandwiched between lesions and ATLOs expressed CXCL13 and CCL21 (Fig. 6 a, top). In contrast, the media of the thoracic aorta of *apoE*$^{-/-}$ mice (Fig. 6 a, bottom), the media of the abdominal aorta of *apoE*$^{-/-}$ mice without adjacent lesions, and the media of the entire aorta of wild-type mice (not depicted) were CXCL13^{-}CCL21^{-} or CXCL13^{dim}CCL21^{-}. CXCL13 and CCL21 colocalized with smooth muscle actin (SMA) and SMA^{dim} myofibroblasts, which may represent dedifferentiated SMCs (Fig. 6 b, top). Both CXCL13 and CCL21 colocalized with VCAM-1, indicating that CXCL13^{+} and CCL21^{+} SMCs were activated (Fig. 6 b, bottom). In addition to media SMCs, fibroblast-like cells with DC morphology in ATLO B cell follicles were CXCL13^{+} (Fig. 6 a), and Lyve1^{+} lymph vessels (L) and larger MECA-32^{+} blood vessels (arrows) in ATLO T cell areas expressed CCL21. Thus, the media separating plaques and ATLOs becomes modified, containing activated SMCs that express the lymphorganogenic chemokines CXCL13 and CCL21. This activation may be an organizing event by which SMCs support the development and maintenance of ATLOs.

SMCs transduce ATLO neogenesis signals through LTβR signaling

As LTβR signaling is required for SLO and TLO formation and CXCL13 expression (15, 23, 28–36), we determined mRNA levels of major *Tnfr* family members in SMCs. Microarrays of LCM-separated media showed a five- to sevenfold

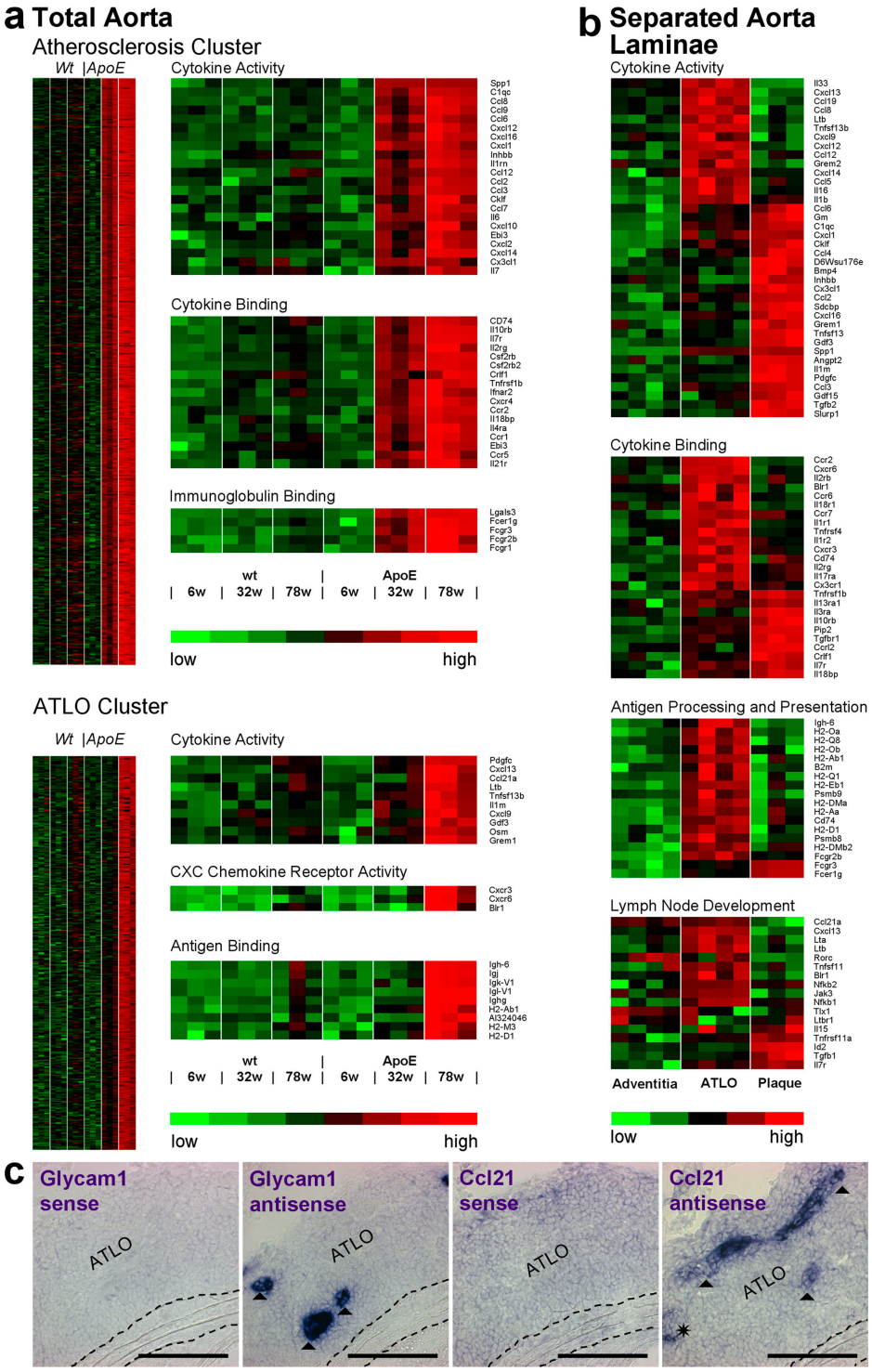

Figure 4. Lifespan aorta gene expression profiling identifies candidate *atherosclerosis versus ATLO* genes. Microarrays were prepared from total aortae of individual mice of each genotype (total aorta in a) or from LCM-derived tissues (separated aorta laminae in b). Differentially regulated probe sets were identified as described in Materials and methods. Probe sets specifying genes with the highest signal strengths are displayed. (a) Atherosclerosis cluster displays genes up-regulated between 6 and 32 wk; heat maps at right indicate significantly up-regulated genes (unpaired Student's *t* test; $P < 0.05$) of GO terms cytokine activity, cytokine binding, and immunoglobulin binding. *ATLO* cluster displays genes up-regulated between 32 and 78 wk; heat maps at right indicate significantly up-regulated genes of GO terms *cytokine activity*, CXC chemokine receptor activity, and antigen binding, (b) Heat maps display LCM preparations of adventitia without plaque or ATLO (left; $n = 4$ mice), ATLOs (adventitia adjacent to intima plaque; middle; $n = 4$ mice), or intima plaques (right; $n = 3$ mice). GO terms for cytokine activity, cytokine binding, antigen processing and presentation, and LN development

enrichment of *vascular SMA α* (*Acta2*), and other media marker genes and microarrays of adventitia showed an excess of *myelin basic protein* (*mbp*) mRNA (Fig. 7 a and Table S3). *Ltbr* and *tumor necrosis factor receptor superfamily, member 1A (Tnfrsf1a)* mRNAs were also strongly expressed in LCM media arrays (Fig. 7 a, Table S3, and not depicted), suggesting that *Ltbr* and *Tnfrsf1a* mRNAs are the major *Tnfr*s expressed by SMCs in vivo. To confirm these findings, we purified SMCs to ≥99% and determined *Ltbr*/*Tnfrsf1a* mRNA levels. Indeed, *Ltbr*/*Tnfrsf1a* represented the major *Tnfr* family members in highly purified aorta SMCs (Fig. 7 b), and SMC cultures maintained this pattern (Fig. 7 c). LTβR- and TNFRSF1A-dependent signaling pathways were examined in SMCs after addition of agonistic anti-LTβR antibody (α-LTβR) or TNF, respectively; α-LTβR, but not TNF, activated the alternative NF-κB pathway, as indicated by p100 to p52 processing and increased RelB DNA binding; TNF, but not α-LTβR, increased p100 protein levels, triggered IκBα degradation, and induced classical RelA DNA binding (unpublished data). Because there is significant cross talk between LTβR and TNFRSF1A in fibroblasts (37), we explored whether α-LTβR and TNF activated *Cxcl13* expression in SMCs. qRT-PCR analysis revealed small effects when each agonist was added alone, but a marked synergistic action of both agonists on *Cxcl13* mRNA induction at 24 h (Fig. 7 d). Thus, SMCs express LTβR and TNFRSF1A as their major TNFR members in vivo, engage the alternative and classical NF-κB signaling pathways, respectively (38), and their combined activation strongly up-regulates *Cxcl13* mRNA (Fig. 7 d) and protein (unpublished data) in SMCs.

Ongoing LTβR signaling is required to maintain ATLO size and structure

Ectopic $LT\alpha_1\beta_2$ or CXCL13 is sufficient to induce TLO formation (27–29, 31, 32, 34, 39, 40). Thus, we treated 75-wk-old $apoE^{-/-}$ mice with an antagonistic LTβR-Ig for 3 wk to assess its effect on ATLOs. As a positive control for LTβR-Ig efficacy, we confirmed that the microarchitecture of the spleen (Fig. 8 a, top), whose structural integrity depends on LTβR (39), was disturbed. After 3 wk, LTβR-Ig had disrupted marginal zone mucosal addressin cell adhesion molecule 1–positive (MAdCAM-1$^+$) structures and eradicated GC FDCs (CD35$^+$) and GC centrocytes (PNA$^+$), and, to a lesser degree, follicular mantle (IgD$^+$) B cells in aged $apoE^{-/-}$ spleens (Fig. 8 a, bottom). LTβR-Ig treatment also markedly disrupted ATLO structure, as shown by a large reduction of B follicle cellularity with minor effects on T cells and plasma cells, a major decrement of ATLO stages (Fig. 8 b), a strong decrease in HEV (PNAd$^+$) incidence (Fig. 8 c), significant reductions of aorta *Cxcl13*, *Glycam1*, and *Il7r* mRNAs (Fig. 8 d), and a moderate attenuation of CXCL13 serum levels (Fig. 8 e).

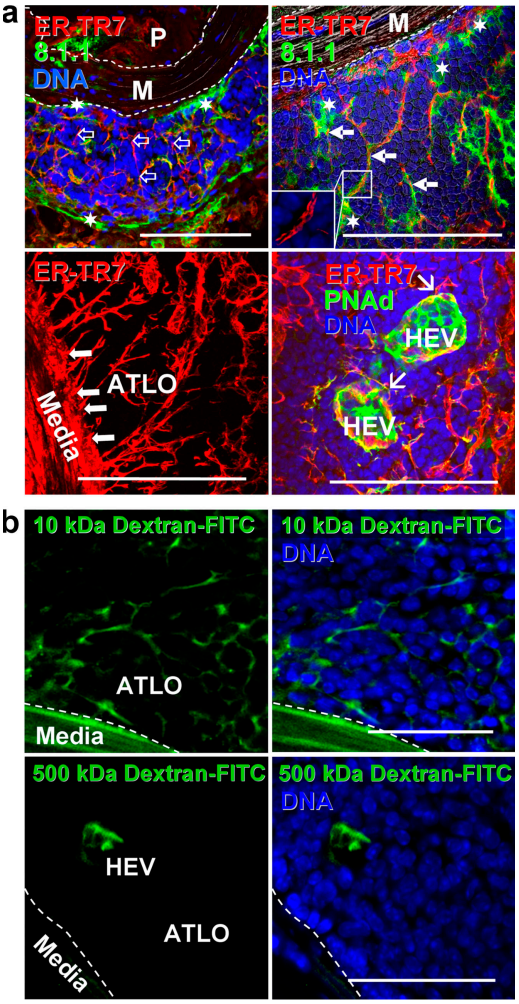

Figure 5. ATLO conduits connect media SMCs with ATLO compartments and facilitate transport of small molecular weight molecules. (a) Conduits connect the media (M) with HEVs. ECM meshwork (ER-TR7; top left, open arrows) associated with (top left, asterisk) and enfolded by 8.1.1$^+$ fibroblastic reticular cells (top right, filled arrows). Conduit pseudolumen (inset, top right). Conduits at the ATLO periphery (ER-TR7) connect the media with HEVs (bottom panels, arrow; Fig. S4 and Video 2; Fig. S5 and Video 3). (b) ATLO conduits transport low molecular weight molecules. 10 or 500 kD fluorescent dextran was injected i.v.; 15 min later, ATLOs were prepared as described in Materials and methods. Dotted lines indicate ATLO/media border. Note presence of 500 kD dextran in HEV (bottom right) and presence of 10 kD, but not 500 kD, dextran in media. Bars, 50 µm.

Although LTβR-Ig attenuates plasma cholesterol levels in $Ldlr^{-/-}$ mice (41), no effect was observed on total cholesterol or on VLDL-, LDL-, or HDL-cholesterol in $apoE^{-/-}$ mice (Fig. S9 and Table S4, available at http://www.jem.org/cgi/content/full/jem.20080752/DC1). Thus, antagonism of LTβR

were examined. (c) *Glycam1* and *Ccl21* mRNA in situ hybridization analyses of ATLO-burdened abdominal aorta segments. Sense and antisense cRNA probes were generated, and in situ hybridization analyses were performed (filled triangle, HEV; asterisk, lymph vessel). Media and lesions did not show specific *Glycam1* or *Ccl21* mRNA signals. Broken lines designate media. Bars, 100 µm.

pathway in *apoE*$^{-/-}$ mice suppresses ATLO maintenance and structure without affecting plasma lipids.

Intima/media and ATLO/media border regions are infiltrated by CD68^{+}CD11c^{+} monocytes/macrophages and T cells and show elastic fiber erosion

Finally, we wondered whether ATLO formation affected the integrity of the aorta, as it has been suggested in humans where B cells within the adventitia of abdominal aortae characterize specimens with aneurysm (42–44). Indeed, ATLOs were associated with leukocyte infiltration, including CD68^{+} cells, of the abdominal aorta in both the outer and inner media layers (Fig. 9 a, left). Elastin staining indicated erosion of the internal lamina and adjacent elastic membranes in association with atherosclerotic plaques (Fig. 9 b, left arrows). In comparison to thoracic aorta, destruction of abdominal aorta media structure was more pronounced (unpublished data). Erosion of the external lamina was observed in association with ATLOs (Fig. 9 b, right arrows).

In addition to CD68, many, but not all, of the infiltrated medial leukocytes were positive for CD11c (Fig. 9 a, right). CD11c expression characterizes Ly6C^{lo} monocytes in blood and of many macrophages in atherosclerotic lesions, but the immediate precursor and functional impact of the CD11c^{+} or CD11c^{-} myeloid cells in lesions and in the media remain to be determined (45). We observed high expression levels of CD11c, CD68, and *Ltb*, but not *VE-cadherin*, mRNAs in LCM media arrays of abdominal aorta that were associated with ATLOs. These data are consistent with immunofluorescent analyses of CD11c^{+} myeloid cells in the inner and outer media of diseased aorta (Fig. 9 a). MECA-32^{+} vasa vasora were observed in advanced plaques (which was, however, a rare event), but not in media with associated plaques. *Ltb* mRNA was highly expressed in sorted blood Ly6C^{lo} monocytes (Fig. 9 c), raising the possibility that the infiltration of this cell type in media may activate SMC LTβR to initiate the formation of ATLOs, which in turn promote elastin erosion that may contribute to aneurysm formation. This possibility, and the mechanism by which SMC LTβR activation occurs, requires in depth testing in future studies.

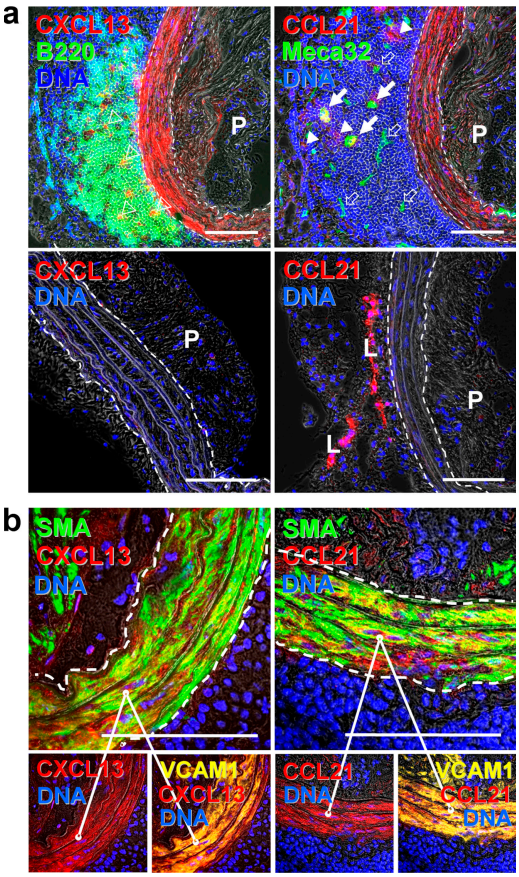

Figure 6. Media SMCs sandwiched between lesions and ATLOs are activated and express the lymphorganogenic chemokines CXCL13 and CCL21. (a) CXCL13 and CCL21 of ATLO-burdened aorta segment (top). Media SMCs and cells with DC morphology stain positive for CXCL13 in B cell follicle (top left, open triangles) and for CCL21 in T cell area (top right, filled arrows), whereas SMCs of aorta segments without adjacent ATLO (thoracic aorta with plaque) do not (bottom). Medium-sized ATLO blood vessels stain positive for CCL21 (top right, filled arrows), whereas small blood vessels (top right, open arrows) in B cell follicles are CCL21^{-}. L, lymph vessel; P, plaque. (b) Colocalization of SMA and CXCL13 and SMA and CCL21 with VCAM-1 in abdominal aorta segments adjacent to ATLO. Bars, 100 µm.

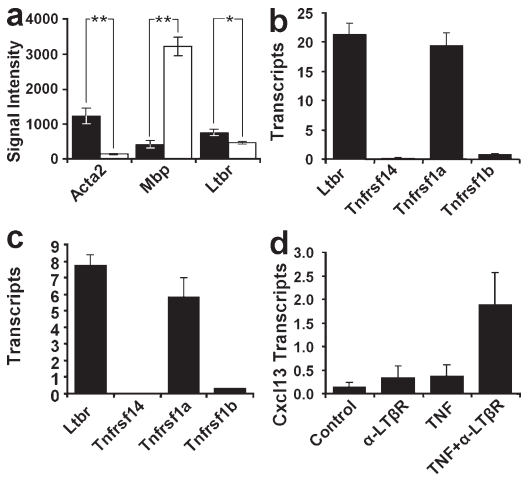

Figure 7. SMCs express LTβR and TNFRSF1A and induce CXCL13 mRNA. (a) Microarray analyses of LCM-derived media (shaded columns) versus adventitia (open columns) from 78-wk-old wild-type mice were examined for signal strengths of *Acta2*, *Mbp*, and *Ltbr*. Means of three independent LCM preparations of individual aortae ± SEM. *, $P < 0.05$; **, $P < 0.001$; two-sided, unpaired Student's *t* test. (b) qRT-PCR analysis of the expression of *Ltbr*, *Tnfrsf14*, *Tnfrsf1a*, and *Tnfrsf1b* expression in freshly isolated SMCs. Means of three independent SMC cultures ± SEM. (c) Same analyses as in b in cultured SMCs. (d) Cultured SMCs were stimulated with 10 µg/ml α-LTβR, 1 ng/ml TNF, or both for 24 h, and *Cxcl13* transcripts were determined by qRT-PCR. Data represent means of five independent experiments ± SEM. $P < 0.05$, one-sided paired Student's *t* test.

DISCUSSION

The structured assembly of lymphocytes in SLOs is a powerful means to amplify immune surveillance (46). SLOs arise during development at predetermined locations, whereas TLOs emerge in adults at diverse sites in response to persistent inflammation, such as in autoimmunity (23, 25, 33, 35,

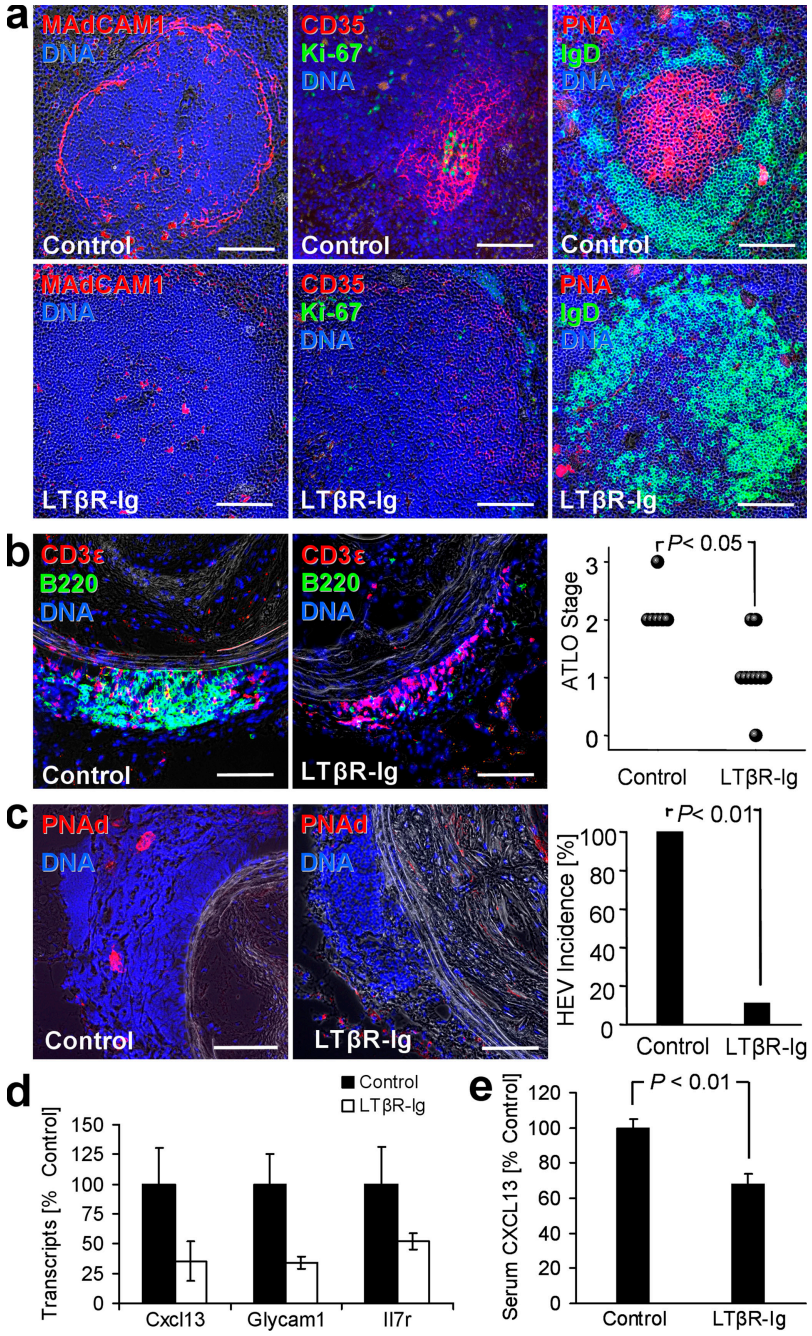

Figure 8. In vivo blockade of LTβR by soluble LTβR-Ig disrupts ATLO structure, reduces *Cxcl13* and *Glycam1* mRNAs, and attenuates serum CXCL13 levels. *ApoE*$^{-/-}$ mice at 75 wk were treated three times with 75 µg LTβR-Ig (n = 11) or the same concentration of human IgG (n = 6) i.p. every 7 d for 3 consecutive weeks. (a) At the end of the treatment period, LTβR-Ig treatment was monitored in the spleen by loss of integrity of marginal zones (MAdCAM-1), FDCs (CD35), cell proliferation (Ki67), centrocytes (PNA), and follicular mantle B cells (IgD); note loss of FDCs and centrocytes and that mantle IgD$^+$ B cells are less affected. (b) ATLO stages were determined after staining with CD3ε (T cells), B220 (B cells), and CD35 antisera (FDC). χ^2 test, P < 0.05. (c) HEVs (PNAd$^+$) abundance was determined by the χ^2 test in LTβR-Ig versus control IgG-treated mice (P < 0.05); representative stainings are shown at left. (d) Aortae of LTβR-Ig– (n = 6) or control IgG-treated (n = 3) mice were examined by qRT-PCR for *Cxcl13* (P < 0.01), *Glycam1* (P < 0.05), and *Il7r* (P < 0.05) mRNAs; unpaired Student's t test; means ± SEM. (e) serum CXCL13 levels of control hu-IgG–treated mice (n = 4) or LTβR-Ig–treated mice (n = 7). Means ± SEM (P < 0.01). Bars, 100 µm.

36, 47–52). Unlike SLOs, TLOs are often accompanied by tissue destruction with progressing clinical symptoms (30, 36, 53–55). Although common forms of atherosclerosis, including coronary heart disease, are recognized chronic inflammatory diseases (1–6), this work is the first to characterize ATLOs associated with this disease in detail. These data in particular provide mechanistic insight into how, where, and when ATLOs form, and our findings also offer insight into possible roles that ATLOs may have in atherosclerosis.

Concerning the mechanisms of ATLO neogenesis, our findings suggest the new concept that medial SMCs translate signals from the overlying atherosclerotic plaques to promote ATLO neogenesis. We show that SMCs beneath atherosclerotic plaques become activated through LTβR and TNFRSF1A signaling to express CXCL13 and CCL21. Indeed, these activated SMCs acquired prototypical features of mesenchymal cells termed lymphoid tissue organizers that were originally described to control embryonic LN development (47). It is well established that certain stromal cells resembling myofibroblasts may differentiate into lymphoid tissue organizers in adult organisms. These lymphoid tissue organizers interact with hyperactivated lymphocytes that are attracted to inflamed tissues and thereby organize TLO neogenesis (25). It is also known that lymphoid tissue organizers can acquire different phenotypes, as seen with activated intestinal fibroblasts in inflammatory bowel disease or activated synoviocytes in rheumatoid arthritis (23, 25, 35). Our findings suggest that SMCs in the aorta adjacent to ATLOs become lymphoid tissue organizers.

The lymphoid organization that they bring about is profound, as the level of cellular and structural organization in

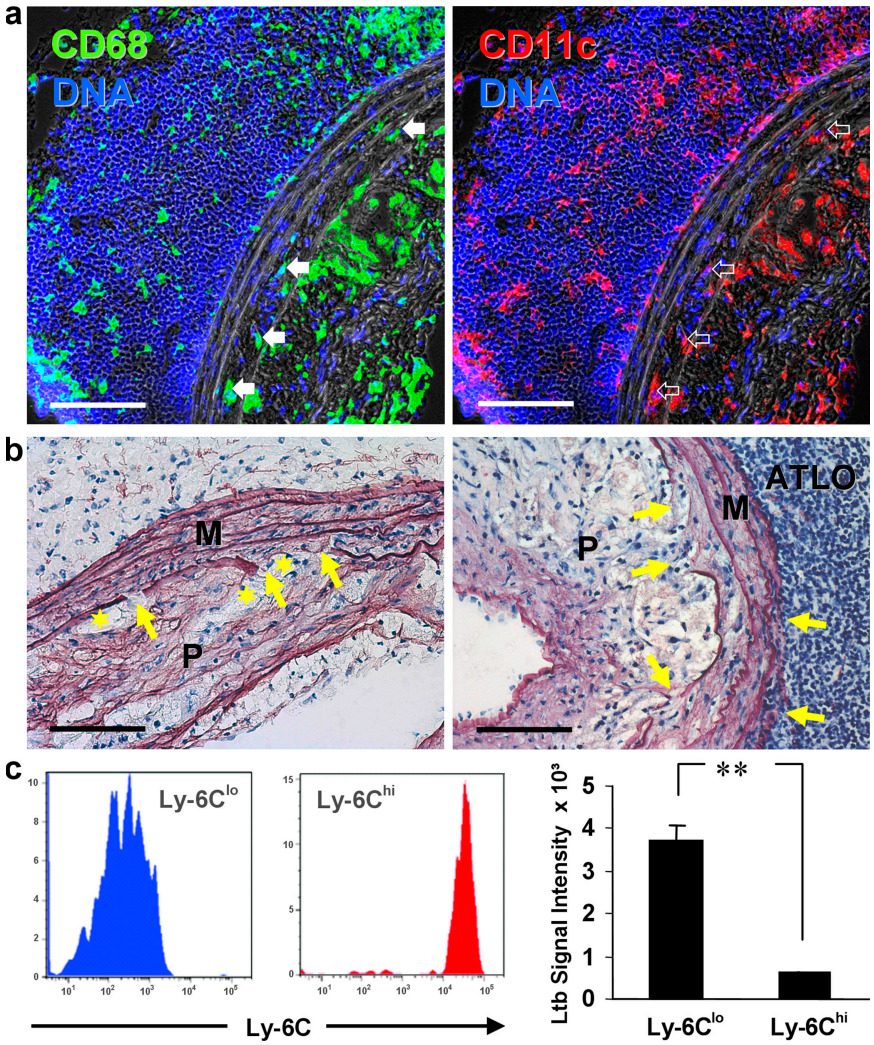

Figure 9. Thoracic and abdominal aorta media of aged *apoE*$^{-/-}$ aorta is infiltrated by leukocytes and shows differential loss of integrity. (a) ATLO staining for CD68^{+} macrophages (left, filled arrows) and CD11c^{+} macrophages/DCs (right, open arrows) show leukocyte infiltration of inner and outer media. (b) Elastin staining of ATLO-free diseased abdominal aorta shows loss of elastic fiber integrity in the inner media (left arrows), whereas ATLO-associated abdominal aorta shows loss of integrity in inner and outer media (right arrows). Foam cells adjacent to media are often associated with elastin strand breaks (asterisks). (c) FACS-sorted blood monocyte subset (left) microarrays (right) reveal differential *Ltb* mRNA expression (two-sided unpaired Student's *t* test; $P < 0.0001$). Bars, 100 µm.

ATLOs was akin to organization previously only observed in LNs and spleen. ATLOs harboured all hematopoietic and nonhematopoietic cell lineages, cell subtypes, and structures that are required to support lymphocyte recruitment and recirculation and to conduct antigen-dependent (auto)immune responses (4–6, 51, 55, 56). These included FDCs, proliferative B cells that were differentiated and organized in follicles, T/B cell interactions in separate T cell areas, two major T reg cell subsets, and plasma cells (Fig. 10). In addition, newly formed conduits establish an elaborate network connecting ATLOs to the medial SMC. This conduit network likely further facilitates and amplifies ongoing communication between ATLOs and the medial SMCs, and possibly overlying plaque, as these conduits could serve as channels for both soluble antigen and transport of molecules (e.g., chemokines, cytokines) between the activated media and ATLOs (20–22). Our findings show that intravenously infused low molecular weight tracers could access and move through the conduits, highlighting their functionality, though the vector of molecular diffusion could not be determined.

An important observation in our analysis was the restriction of ATLOs to the abdominal aortae of aged *apoE*$^{-/-}$ mice. Interestingly, it is the area of ATLO formation where abdominal aorta aneurysms (AAAs) preferentially form in mice (9, 10) and humans (8, 42, 43), raising the possibility that ATLOs are linked in some way to AAA. Leukocyte infiltrates have been associated with AAA, but the importance of T or B cells is still controversial (42, 57–59). Because we

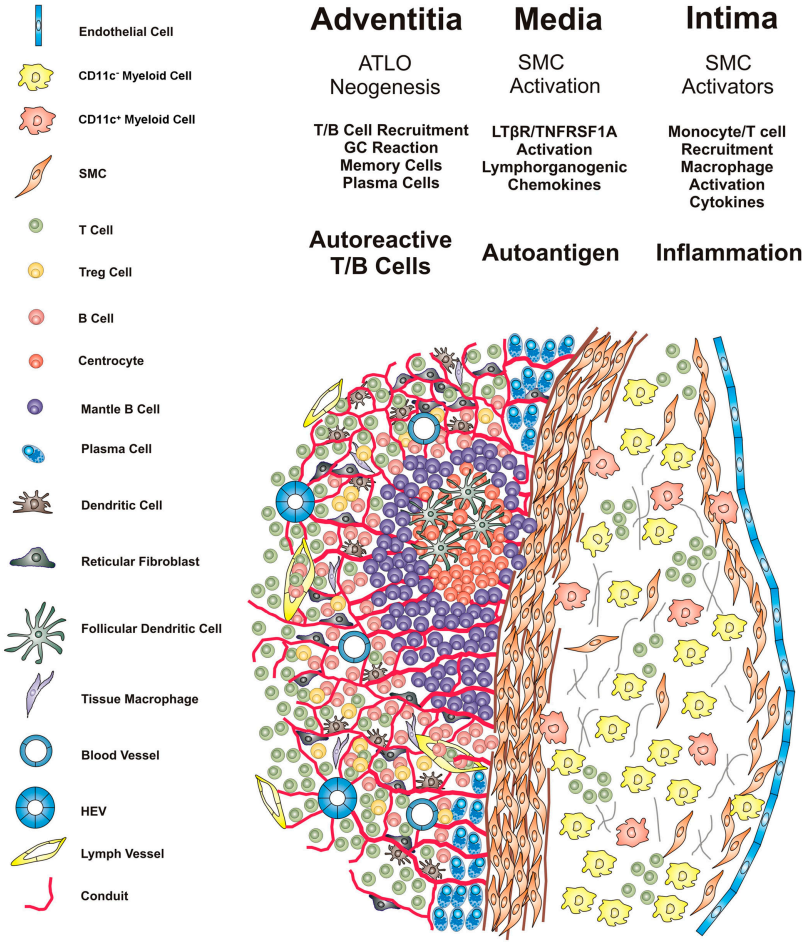

Figure 10. Schematic choreography of cells and molecules in ATLO neogenesis. Blood monocytes/macrophages/foam cells, T cells, and SMCs form atherosclerotic lesions in the intima and initiate a transmural arterial wall inflammation pathway. Lesion cells such as CD11c^{+} and/or CD11c^{-} myeloid cells and T cells produce TNFR agonists LTβ and TNF and, after LTβR/TNFRSF1A activation and induction of alternative and classical NF-κB signaling pathways, media SMCs are activated and acquire features of lymphoid tissue organizers. Lymphorganogenic CXCL13/CCL21 and other mediators gain access to cells residing in the adventitia, recruit B and T cells through vasa vasora, and promote lymphocyte and stromal cell activation. A tissue microenvironment is then generated that induces conduit neogenesis via stimulation of reticular fibroblasts, DC recruitment, HEV formation, ectopic lymph vessel, and blood vessel neogenesis. ATLO formation accelerates and lymphocyte recirculation is markedly facilitated, B cell follicles form, and T reg cells in T cell areas are recruited. Transmural inflammation also generates autoantigen(s), although their nature, transport routes, and functional roles all remain to be defined. Accelerated B cell recruitment leads to B cell follicle formation, and ectopic GCs are activated. Autoantigen-binding FDCs initiates B cell proliferation, differentiation, and affinity maturation. Memory cells and/or plasma cells, and possibly autoreactive T/B cells, together with T reg cell deficiency may lead to clinically apparent and overt autoimmunity and arterial wall pathology.

observed elastic fiber erosion adjacent to ATLO-associated media, we speculate that B cell and/or T cell aggregates in the adventitia of abdominal aortae may contribute to atherosclerosis and AAA pathology. In this context, our findings suggest that *apoE*$^{-/-}$ mice may serve as a suitable animal model that recapitulates similar events in the human abdominal aorta.

Though B cell follicles were prominent in the adventitia of aged *apoE*$^{-/-}$ mice, we did not find a high rate of B cell trafficking into the adventitia after adoptive transfer of splenic B cells. It is possible that B cells in the adventitia may expand locally in response to aortic wall antigens. The ongoing GC reactions in ATLOs support this possibility, and from the limited work in human coronary arteries, we anticipate that the range of B cell clones in the adventitia may be broad (43). Nonetheless, ATLO GC reactions may control antigen-dependent affinity maturation similar to the TLO GC B cell progeny of rheumatoid arthritis patients (13, 14, 23, 50, 52, 60). Although innate B cells appear to be atheroprotective (1–6), it remains possible that autoreactive B cells (61) may be generated during later stages of the disease and contribute to plaque growth and/or AAA pathology.

With regard to the ATLO T cell compartment, it was remarkable to observe that a substantial proportion of ATLO T cells were regulatory in nature, with abundant populations of two major T reg cell subsets. Given indications that Foxp3$^+$ T reg cells are atheroprotective (16), it is tempting to suggest that ATLO T reg cells confer a benefit to the host, but the veracity of this idea remains to be determined. Furthermore, it will be important to determine if the disproportionate number of T reg cells in the adventitial infiltrates holds true in all adventitial leukocyte accumulations, including those more diffuse T cell infiltrates that occur before or without accompanying B cells. The surprisingly high percentage of T reg cells in ATLOs versus the more diffuse infiltrate in the thoracic aorta (10) suggests that both T reg cell subsets home into or proliferate within ATLOs subsequent to the formation of the diffuse T cell–dominated infiltrate of the thoracic aorta. It will also be important in future work to determine if the substantial recirculation of T cells into the adventitia compared with that of B cells in our adoptive transfer studies was limited to a large proportion of T reg cells or whether T reg cells particularly expanded in situ. Because the treatment of *apoE*$^{-/-}$ mice with LTβR-Ig greatly reduced HEV abundance, and because HEVs in turn mediate T cell recruitment into ATLOs, our data imply that continuous LTβR activation maintains a high rate of aorta T cell recirculation. Thus, manipulation of the LTβR pathway may be one means to regulate the accumulation of T cells, including T reg cells in diseased arteries.

An unresolved issue requiring further investigation is the source of ligand to activate LTβR signaling in medial SMCs. The presence of CD11c$^+$CD68$^+$ cells in the media between ATLOs and atherosclerotic plaques led us to consider the possibility that CD11c$^+$CD68$^+$ Ly6C^{lo} monocytes that accumulate in atherosclerotic plaques might be a source of the signal (45, 62). In agreement with this possibility, we found that Ly6C^{lo} monocytes expressed higher levels of LTβ compared with more classical Ly6C^{hi} monocytes. Studies to manipulate LTβ expression selectively in these monocytes would help to determine whether they serve as the source of activating signal in the induction of ATLOs through SMC activation.

A major issue raised by our data relates to the functional impact of ATLOs on atherosclerosis. It is not surprising that the short treatment period of severely diseased and aged *apoE*$^{-/-}$ mice with LTβR-Ig failed to significantly reverse or aggravate the disease in standard atherosclerosis assays (unpublished data). To circumvent this limitation, it may be valuable to generate *apoE*$^{-/-}$ mice with tissue-selective deletion of the LTβR in SMCs or deletion of LTβ in leukocytes subsets known to affect TLOs (32, 34). While these experiments are underway, our data encourage reexamination of the roles of immune cell subsets in advanced stages of atherosclerosis as opposed to early stages (1–6). As pointed out above, most studies in mice have focused on the early stages of atherosclerosis (6), when autoreactive T and B cells (63) may not yet have had the opportunity to be fully activated (61). That natural T reg cells and the CD137/CD137L pair (which are both implicated in the regulation of tolerance and autoimmunity) control the development of atherosclerosis was recently demonstrated in hyperlipidemic mice (16, 64), and here we have identified two T reg cell subsets in ATLOs. It is well established that autoimmune diseases develop in clinically separable phases and only in their late stages, when tolerance toward autoantigen(s) is breaking down, do they convert to explicit self-reactivity associated with debilitating tissue destruction. Similar multistage immune responses may occur in atherosclerosis. Clinically overt disease such as myocardial infarction is a late event triggered by plaque rupture and endothelial cell erosion. It will be of considerable interest to examine the possibility that these events are caused by autoreactive T- and/or B cells and/or autoantibodies, as well as dysfunction of T reg cells on the diseased arterial wall (1–6).

Finally, our data should help to advance experiments in aged *apoE*$^{-/-}$ mice to test the efficacy of pharmaceuticals that have been developed to treat autoimmune disorders. These pharmaceuticals range from clinically effective therapies for rheumatoid arthritis, including several anti–B cell–based pharmaceuticals to preclinical pharmaceuticals that target plasma cells or disrupt T–B cell help (50).

MATERIALS AND METHODS

Mice. Mice on the C57BL/6J background were purchased from The Jackson Laboratory. Mice were housed in a specific pathogen–free environment on a 12-h light/dark cycle and fed a standard rodent chow (Altromin). Animal procedures were approved by the Animal Care and Use Committee of Thuringia. Treatment of aged apoE$^{-/-}$ mice by soluble (decoy) LTβR–Igis was as follows: 75-wk-old *apoE*$^{-/-}$ mice were treated by 3 weekly i.p. injections of 75 μg LTβR-Ig or 75 μg control human serum IgG (Gamunex 10%; Bayer Vital) as control. 1 wk after the third application, animals were killed and aortae were dissected. The aorta was perfused in situ and care was taken to preserve the adventitia. For qRT-PCR and microarray analyses, aortae

were dissected at 8°C without adherent adipose tissue. We found that treatment of young apoE$^{-/-}$ mice on a cholesterol diet by LTβR–Ig does not affect plasma lipids. Independent colonies of *Ldlr*$^{-/-}$ and *apoE*$^{-/-}$ mice were studied at the University of Chicago, and lipid levels were determined as previously described (65). These 8-wk-old mice were maintained on a high cholesterol (Western) diet for 12 wk in the absence or presence of LTβR-Ig.

Morphometry, histology, and immunohistochemistry. Tissues were embedded in Tissue Tec (Sakura Finetek) and stored at −80°C. 10-µm cross sections were prepared, and every 10th section was stained with Oil Red O/hematoxylin. Eight consecutive Oil Red O–stained sections of the aortic arch/innominate artery and the abdominal aorta distal to the *A. renalis* were used to quantify atherosclerosis and corresponding ATLO sizes. Tissue areas were determined using Leica Q500/W software. Elastic fibers were stained with Unna-Taenzer orcein stain. Fluorescence immunohistology was performed as previously described (9, 10), using marker antibodies CD68 (macrophages; Serotec, Ltd.), CD3ε (T lymphocytes; 145-2C11; BD), CD45R/B220 (B lymphocytes; BD), CD35/CD21b (CR1, FDCs; BD), MECA-79 (PNAd carbohydrate epitope in HEV; BD), MECA-32 (panendothelial cell antigen; BD), MAdCAM-1 (MECA-367; BD), Ki67 (M-19; Santa Cruz Biotechnology, Inc.), LYVE-1 (lymphatics; Acris), ER-TR7 (reticular fibroblasts; BMA), 8.1.1 (gp38, podoplanin; Acris), CD138 (syndecan-1; BD), CXCL13 (BLC; R&D Systems), CCL21 (SLC; R&D Systems), IgD (11-26c.2a; BD). DAPI was used to stain DNA. Secondary antibodies were as previously described (9, 10). FITC-labeled PNA (Vector Laboratories) was used to stain centrocytic B cells. TLOs in atherosclerotic aortae of mice were classified into developmental stages, as described in Fig. S1.

Flow cytometry. Digests from similarly sized diseased portions of thoracic or abdominal aortae were prepared as previously described (11). After digestion, cell suspensions were filtered through a 70-µm cell strainer and centrifuged. Cell pellets were resuspended in PBS containing 2% FCS and pretreated with purified anti–mouse CD16/32 mAb at a concentration of 0.5 µg/10^6 cells for 10 min on ice to block Fc receptor binding. Without washing, cells were incubated with mAbs for 25 min at 4°C, washed twice, and, when required, incubated with secondary mAbs or streptavidin conjugates for an additional 20 min. After washing, samples were analyzed with a FACSCalibur or a FACSCantoII using CellQuest Pro or FACSDiva software (BD). The following mAbs were used: CD45-PE-Cy7 (clone 30-F11), TCRβ-FITC or -Biotin (H57-597), CD4-PE or -APC (GK1.5), CD8α-Pacific blue (53–6.7), CD28-Biotin (37.51), CD69-PE (H1.2F3), CD44-APC (1M7), CD16/32 purified (93), and CD115-Biotin (AFS98; all from eBioscience); CD19-APC (1D3), CD11b-FITC (M1/70), CD25-FITC (7D4), NK1.1-FITC (PK136), Gr-1-APC (RB6-8C5, reacts with Ly-6C), appropriate IgG isotype controls, and Streptavidin-PerCP-Cy5.5 or -PerCP (all from BD); and F4/80-FITC (CI:A3-1; AbD Serotec). Intracellular Foxp3 staining was performed with the anti–mouse-Foxp3-PE (FJK-16s) staining kit (eBioscience) according to the manufacturer's instructions. Monocyte subsets were purified with a FACSAria cell sorter (BD) based on forward and sideward characteristics and marker antigen expression, as previously described (45). Ly-6C^{hi} monocytes were sorted as CD115$^+$F4/80$^+$Gr-1^{hi} and Ly6C^{lo} monocytes were sorted as CD115$^+$F4/80$^+$Gr-1^{lo}.

SMC purification. SMCs were obtained from aortae of C57BL/6 mice by sequential dissection, careful removal of adventitial tissue and endothelial cells, and collagenase/elastase (Worthington Biochemical Corporation; Sigma-Aldrich) digestion (66). Purity of SMCs was ≥99%, as shown by α-SMA positivity of cytospins.

Tracer analyses. Fluorescein-conjugated, lysine-fixable dextrans (Invitrogen) were injected i.v. in 200 µl at 5 mg/ml (10 kD) and 2 mg/ml (500 kD). 15 min later, aorta, LNs, and spleen were removed and fixed for 3 h in 4% paraformaldehyde in PBS. Tissues were washed in PBS and incubated overnight at 4°C in 20% sucrose/PBS before freezing in Tissue-Tek (Sakura Finetek).

qRT-PCR. RNAs were extracted with Trizol (Invitrogen) and purified using RNeasy Micro kit (QIAGEN). RNA integrity was determined on RNA 6000 Nano LabChips (Agilent Technologies). qRT-PCR was performed as previously described (10). Specificity of primers was confirmed by melting curve analyses and product sequencing. Forward and reverse primers were as follows *Actb*, 5′-GCTCCATCCTGGCCTCACTGT-3′, 3′-GAAAGGGTGTAAAACGCAGCTCA-5′ (136 bp); *Ltb*, 5′-GAGACAGTCACACCTGTTG-3′; 3′-CCTGTAGTCCACCATGTCG-5′ (141 bp); *Ltbr*, 5′-TGGTGCTCATCCCTACCTTC-3′, 3′-TCCCAAACTCTCCTCCACAC-5′ (181 bp); *Tnfrsf14*, 5′-TCCATCCTTTTGCCACTTGTGA-3′, 3′-CTGTCTCCTCCTCGGTCTCAGC-5′ (181 bp); *Tnfrsf1a*, 5′-CGATAAAGCCACACCCACAACC-3′, 3′-TGGTACATCTCCCTGCCACTCA-5′ (223 bp); *Tnfrsf1b*, 5′-GGCAGAGGAGCCTAGTTGTTGC-3′, 3′-ATCCACACAAGCACAGGAGCTG-5′ (238 bp); *Ccl21*, 5′-ATCCCGGCAATCCTGTTCTT-3′, 3′-AGTTCTCTTGCAGCCCTTGG-5′ (201 bp); *Cxcl13*, 5′-TCCTGGGAAGCTGGTGCAATG-3′, 3′-TCATCAGGGTCACAGTGCAAAGG-5′ (216 bp); *Glycam1*, 5′-CCAAGTCAAGCCAGACAGTGGA-3′, 3′-GCAGACTGAGAGGTGGTGGTCA-5′ (196 bp); *Il7r*, 5′-TGCGCACACCACAATGAGTGC-3′, 3′-TGACCGGACAGACACTCCAATCC-5′ (247 bp). *ELISA*. CXCL13 ELISA was performed as recommended by the supplier (R&D Systems).

Cell culture. SMCs were maintained in DMEM/F12/10% FCS (Invitrogen) and used at passages 1–3. For qRT-PCR analyses, cells were stimulated with 10 µg/ml agonistic rat anti–mouse α-LTβR mAb 5G11b (67) or 1 ng/ml mouse recombinant TNF (R&D Systems) as indicated in the figure legends.

Microarray analysis. Aorta microarray analyses were performed as previously reported (68, 69). 3 wild-type and *apoE*$^{-/-}$ mice each at 6, 32, and 78 wk or LCM-derived aorta tissues at 78 wk were used. Signal intensities were calculated from the raw data and scaled to an array trimmed mean of 500. All further steps were performed using R and Bioconductor. Logarithmized signals were normalized across arrays using quantile normalization (70), and data were filtered before statistical analysis to remove genes with low expression or without variability between mouse groups at 6 and 78 wk. Probe sets were included if in one group a minimum of 2 arrays was called present (detection $P \leq 0.05$) and 2 or 3 arrays showed a log signal ≥log2(200). Recorded genes were required to be up-regulated from 6–78 wk with a fold change of at least log2(2.5). Using the data from the three *apoE*$^{-/-}$ groups, the resulting list was subjected to a one-factor analysis of variance with Benjamini and Hochberg correction for multiple testing (71). 1,163 probe sets were significantly differentially expressed ($P \leq 0.05$) and used for further analyses (Table S1).

Cluster analysis. Group means of the selected probe sets were standardized to zero mean and unit variance (72). A fuzzy c-means algorithm was applied with the euclidean metric and fuzzy parameter FP = 1.2. Using the maximum-membership function, hard cluster assignments were identified for the best out of 30 runs of the fuzzy c-means algorithm with random initial partitions (73). Data were used to exploit the different time windows of atherosclerosis formation and ATLO development. For this purpose, each probe set of a presumed atherosclerosis cluster was required to show significant up-regulation between 6 and 32 wk (Fig. 4 a, Table S1, and Fig. S4), whereas each probe set of a presumed ATLO cluster was required to show significant up-regulation between 32 and 78 wk (Fig. 4 a, Table S1, and Fig. S4 B). This approach ascertained that genes that were up-regulated between 6 and 32 wk were segregated from genes that were newly appearing during the time window 32 to 78 wk. GO molecular function terms in both clusters confirmed the marked expression of macrophage/inflammation genes in the atherosclerosis cluster whereas the ATLO cluster showed preferential expression of B cell immunity and adaptive immune-effector genes (Fig. 4 and Table S1). Although many genes in each cluster have multiple biological functions depending on their tissue-specific expression and local biology, these data provide preliminary evidence that the atherosclerosis cluster contained genes that largely represent the influx of blood-derived monocytes into the arterial wall intima, including multiple inflammation-regulating genes, whereas the ATLO cluster contained genes known to regulate embryonic LN development and TLO formation with a major overrepresentation component of

genes regulating B cell maturation, GC formation, plasma cells (immunoglobulin genes), autoimmunity, and affinity maturation (Fig. 4). Selected transcripts were confirmed by quantitative RT-PCR (Fig. S5).

LCM procedure. LCM was performed using a Palm MicroBeam laser system (PALM Microlaser Technologies AG) according to published procedures (74–76) with slight modifications. 10 sections (10 µm) of the abdominal aorta were placed on cooled PEN membrane-covered glass slides (PALM Industries). Slides were dried 10 min at 45°C and stored in an exsiccator. Approximately 200 unstained sections for each arterial wall compartment/array were obtained. Each section was collected from the membrane and transferred to Trizol (Invitrogen). RNA was extracted and purified using RNeasy Micro kit (QIAGEN). As a first step to ascertain reproducibility, RNA integrity, validity, and reliability of our LCM protocol, we established protocols to obtain various aorta arterial wall compartments. Unstained phase contrast images of 10 µm serial fresh-frozen tissue sections showed that the media/adventitia border (and for diseased arteries in *apoE*$^{-/-}$ mice, the media/atherosclerotic intima lesion border) could be readily identified before immunohistochemical staining caused by contrast-rich elastin fibers in the media. This allowed us to omit immunofluorescence staining before LCM. These data provide comprehensive information on media SMC gene expression of constitutively expressed genes (GEO accession no. GSE10000).

Adoptive transfer experiments. Lymphocyte recirculation assays were done as previously described, with minor modifications (19). In brief, total splenocytes were isolated from 12-wk-old male C57BL/6J mice, and erythrocytes were treated with lysis buffer (QIAGEN). Cells were labeled with 5 µM CFSE (carboxyfluorescein diacetate succinimidyl ester) for 10 min at room temperature according to the manufacturer's protocol (Invitrogen). After washing, up to 35×10^6 CFSE-labeled cells were injected into the tail vein of 40- or 90-wk-old *apoE*$^{-/-}$ mice. 3 or 18 h after cell transfer, recipient mice were killed and whole aorta with adjacent LNs (i.e., renal, caudal, lumbar, and inguinal LNs) were cryo-preserved. Sections were analyzed by confocal laser scanning microscopy at 18 h when > 90% of blood CFSE$^+$ cells had left the circulation. To reduce unspecific autofluorescence of lipid deposits of the plaque region, LSM510 software was used. For this purpose two laser lines were applied separately to the same specimen. The first laser (488 nm) detected CFSE-specific signals as well as autofluorescence, and the second unrelated laser (543 nm) was used to visualize unspecific autofluorescence.

In situ hybridization. In situ hybridization was performed on cryostat tissue sections as previously described (77), with slight modifications. In brief, cDNA fragments were amplified using the primers 5′-ATCCCGGCAATCCTGTTCTT-3′, 5′-AGTTCTCTTGCAGCCCTTGG-3′ (*Ccl21a*) and 5′-CCAAGTCAAGCCAGACAGTGGA-3′, 5′-GCAGACTGAGAGGTGGTGGTCA-3′ (*Glycam1*) and cloned using the TOPO Cloning kit (Invitrogen). Digoxigenin (Roche) labeled cRNAs were applied to each section and hybridized at 65°C overnight. Tissue sections were rinsed as described in the Supplemental text (available at http://www.jem.org/cgi/content/full/jem.20080752/DC1). For color reaction, slides were incubated with BM-Purpel/Levamisol/Tween.

Statistical analyses. Measurements are expressed as means of *n* samples ± SEM. Data were analyzed by two-tailed unpaired Student's *t* test, Pearson correlation, and Chi-Square test, as stated in figure legends using SPSS software (SPSS).

Online supplemental material. Fig. S1 shows ATLO stage classification. Fig. S2 shows that ATLOs are distinguished from paraaortic LNs by shape, structure, and location. Fig. S3 and Video 1 show that transferred CFSE$^+$ splenocytes are associated with HEVs, but not with blood vessel lumina. Fig. S4 shows *early* atherosclerosis cluster versus *late* ATLO cluster. Fig. S5 shows qRT-PCR of selected genes of the adaptive immune response in 32 and 78 wk wild-type and *apoE*$^{-/-}$ aortae. Fig. S6 is an overview of ATLO conduit structure revealed by ER-TR7. Fig. S7 and Video 2 show that conduits connect the media SMC compartments with various ATLO structures. Fig. S8 and Video 3 show that conduits access HEVs. Fig. S9 shows extended LTβR-Ig treatment does not affect total plasma cholesterol or lipoprotein-cholesterol levels in *apoE*$^{-/-}$ mice. Table S1 lists probe sets of *apoE*$^{-/-}$ aorta up-regulated between 6 and 32 wk for atherosclerosis cluster and ATLO cluster. Table S2 shows LCM-derived ATLO and atherosclerosis lesion gene expression. Table S3 shows marker genes and Tnfr family member genes in LCM microarrays of wild-type abdominal aorta media and adventitia. Table S4 shows serum lipid values in aged *apoE*$^{-/-}$ mice maintained on normal mouse chow treated with LTßR-Ig or control hu-IgG. There is also supplemental text. Online supplemental material is available at http://www.jem.org/cgi/content/full/jem.20080752/DC1.

We thank G. Weber, M. Voigt, and S. Noßmann for mouse preparations and morphometry; C. Ströhl for microarray analyses; M. Franke for qRT-PCR analyses; B. Lemser for Western blots, SMC cultures, and mouse dissection; K. Bonhagen for help with cell sorting; N. John and B. Kaiser for mouse dissection and CXCL13 ELISA; and A. Kirsch for art work.

This work was supported by the German Research Organization (HA 1083/15-1/HA1083/13-3; LO1467/1-1 WE2224/5) to A.J.R. Habenicht, K. Lotzer, D. Hu, and F. Weih; by the German BMBF (grant 031270D) to D. Radke; by the Netherlands Organization for Scientific Research (grant 918.56.612) to R.E. Mebius; and the National Institutes of Health (grant 1 RO1HL085516) to G.S. Getz.

The authors declare that they have no competing financial interests.

Submitted: 8 April 2008
Accepted: 10 December 2008

REFERENCES

1. Lusis, A.J. 2000. Atherosclerosis. *Nature*. 407:233–241.
2. Glass, C.K., and J.L. Witztum. 2001. Atherosclerosis. The road ahead. *Cell*. 104:503–516.
3. Libby, P. 2002. Inflammation in atherosclerosis. *Nature*. 420:868–874.
4. Witztum, J.L. 2002. Splenic immunity and atherosclerosis: a glimpse into a novel paradigm? *J. Clin. Invest*. 109:721–724.
5. Wick, G., M. Knoflach, and Q. Xu. 2004. Autoimmune and inflammatory mechanisms in atherosclerosis. *Annu. Rev. Immunol*. 22:361–403.
6. Hansson, G.K. 2005. Inflammation, atherosclerosis, and coronary artery disease. *N. Engl. J. Med*. 352:1685–1695.
7. Schwartz, C.J., and J.R. Mitchell. 1962. Cellular infiltration of the human arterial adventitia associated with atheromatous plaques. *Circulation*. 26:73–78.
8. Houtkamp, M.A., O.J. de Boer, C.M. van der Loos, A.C. van der Wal, and A.E. Becker. 2001. Adventitial infiltrates associated with advanced atherosclerotic plaques: structural organization suggests generation of local humoral immune responses. *J. Pathol*. 193:263–269.
9. Zhao, L., M.P. Moos, R. Grabner, F. Pedrono, J. Fan, B. Kaiser, N. John, S. Schmidt, R. Spanbroek, K. Lotzer, et al. 2004. The 5-lipoxygenase pathway promotes pathogenesis of hyperlipidemia-dependent aortic aneurysm. *Nat. Med*. 10:966–973.
10. Moos, M.P.W., N. John, R. Grabner, S. Nossmann, B. Gunther, R. Vollandt, C.D. Funk, B. Kaiser, and A.J.R. Habenicht. 2005. The lamina adventitia is the major site of immune cell accumulation in standard chow-fed apolipoprotein E-deficient mice. *Arterioscler. Thromb. Vasc. Biol*. 25:2386–2391.
11. Galkina, E., A. Kadl, J. Sanders, D. Varughese, I.J. Sarembock, and K. Ley. 2006. Lymphocyte recruitment into the aortic wall before and during development of atherosclerosis is partially L-selectin dependent. *J. Exp. Med*. 203:1273–1282.
12. Dal Canto, A.J., P.E. Swanson, A.K. O'Guin, S.H. Speck, and H.W. Virgin. 2001. IFN-gamma action in the media of the great elastic arteries, a novel immunoprivileged site. *J. Clin. Invest*. 107:R15–R22.
13. Kosco-Vilbois, M.H. 2003. Are follicular dendritic cells really good for nothing? *Nat. Rev. Immunol*. 3:764–769.
14. Allen, C.D., T. Okada, H.L. Tang, and J.G. Cyster. 2007. Imaging of germinal center selection events during affinity maturation. *Science*. 315:528–531.

15. Furtado, G.C., T. Marinkovic, A.P. Martin, A. Garin, B. Hoch, W. Hubner, B.K. Chen, E. Genden, M. Skobe, and S.A. Lira. 2007. Lymphotoxin beta receptor signaling is required for inflammatory lymphangiogenesis in the thyroid. *Proc. Natl. Acad. Sci. USA.* 104:5026–5031.
16. Ait-Oufella, H., B.L. Salomon, S. Potteaux, A.K. Robertson, P. Gourdy, J. Zoll, R. Merval, B. Esposito, J.L. Cohen, S. Fisson, et al. 2006. Natural regulatory T cells control the development of atherosclerosis in mice. *Nat. Med.* 12:178–180.
17. Ford, M.S., K.J. Young, Z. Zhang, P.S. Ohashi, and L. Zhang. 2002. The immune regulatory function of lymphoproliferative double negative T cells in vitro and in vivo. *J. Exp. Med.* 196:261–267.
18. Zhang, D., W. Yang, N. Degauque, Y. Tian, A. Mikita, and X.X. Zheng. 2007. New differentiation pathway for double-negative regulatory T cells that regulates the magnitude of immune responses. *Blood.* 109: 4071–4079.
19. Cupedo, T., W. Jansen, G. Kraal, and R.E. Mebius. 2004. Induction of secondary and tertiary lymphoid structures in the skin. *Immunity.* 21: 655–667.
20. Nolte, M.A., J.A. Belien, I. Schadee-Eestermans, W. Jansen, W.W. Unger, N. van Rooijen, G. Kraal, and R.E. Mebius. 2003. A conduit system distributes chemokines and small blood-borne molecules through the splenic white pulp. *J. Exp. Med.* 198:505–512.
21. Sixt, M., N. Kanazawa, M. Selg, T. Samson, G. Roos, D.P. Reinhardt, R. Pabst, M.B. Lutz, and L. Sorokin. 2005. The conduit system transports soluble antigens from the afferent lymph to resident dendritic cells in the T cell area of the lymph node. *Immunity.* 22:19–29.
22. Itano, A.A., and M.K. Jenkins. 2003. Antigen presentation to naive CD4 T cells in the lymph node. *Nat. Immunol.* 4:733–739.
23. Aloisi, F., and R. Pujol-Borrell. 2006. Lymphoid neogenesis in chronic inflammatory diseases. *Nat. Rev. Immunol.* 6:205–217.
24. Luster, A.D. 1998. Chemokines–chemotactic cytokines that mediate inflammation. *N. Engl. J. Med.* 338:436–445.
25. Cupedo, T., and R.E. Mebius. 2005. Cellular interactions in lymph node development. *J. Immunol.* 174:21–25.
26. Charo, I.F., and R.M. Ransohoff. 2006. The many roles of chemokines and chemokine receptors in inflammation. *N. Engl. J. Med.* 354:610–621.
27. Luther, S.A., T. Lopez, W. Bai, D. Hanahan, and J.G. Cyster. 2000. BLC expression in pancreatic islets causes B cell recruitment and lymphotoxin-dependent lymphoid neogenesis. *Immunity.* 12:471–481.
28. Alimzhanov, M.B., D.V. Kuprash, M.H. Kosco-Vilbois, A. Luz, R.L. Turetskaya, A. Tarakhovsky, K. Rajewsky, S.A. Nedospasov, and K. Pfeffer. 1997. Abnormal development of secondary lymphoid tissues in lymphotoxin beta-deficient mice. *Proc. Natl. Acad. Sci. USA.* 94:9302–9307.
29. Endres, R., M.B. Alimzhanov, T. Plitz, A. Futterer, M.H. Kosco-Vilbois, S.A. Nedospasov, K. Rajewsky, and K. Pfeffer. 1999. Mature follicular dendritic cell networks depend on expression of lymphotoxin β receptor by radioresistant stromal cells and of lymphotoxin β and tumor necrosis factor by B cells. *J. Exp. Med.* 189:159–168.
30. Ettinger, R., S.H. Munson, C.C. Chao, M. Vadeboncoeur, J. Toma, and H.O. McDevitt. 2001. A critical role for lymphotoxin- β receptor in the development of diabetes in nonobese diabetic mice. *J. Exp. Med.* 193: 1333–1340.
31. Futterer, A., K. Mink, A. Luz, M.H. Kosco-Vilbois, and K. Pfeffer. 1998. The lymphotoxin beta receptor controls organogenesis and affinity maturation in peripheral lymphoid tissues. *Immunity.* 9:59–70.
32. Browning, J.L., N. Allaire, A. Ngam-Ek, E. Notidis, J. Hunt, S. Perrin, and R.A. Fava. 2005. Lymphotoxin-beta receptor signaling is required for the homeostatic control of HEV differentiation and function. *Immunity.* 23:539–550.
33. Cyster, J.G. 2003. Lymphoid organ development and cell migration. *Immunol. Rev.* 195:5–14.
34. Drayton, D.L., X. Ying, J. Lee, W. Lesslauer, and N.H. Ruddle. 2003. Ectopic LTαβ directs lymphoid organ neogenesis with concomitant expression of peripheral node addressin and a HEV-restricted sulfotransferase. *J. Exp. Med.* 197:1153–1163.
35. Drayton, D.L., S. Liao, R.H. Mounzer, and N.H. Ruddle. 2006. Lymphoid organ development: from ontogeny to neogenesis. *Nat. Immunol.* 7:344–353.
36. Lee, Y., R.K. Chin, P. Christiansen, Y. Sun, A.V. Tumanov, J. Wang, A.V. Chervonsky, and Y.X. Fu. 2006. Recruitment and activation of naive T cells in the islets by lymphotoxin beta receptor-dependent tertiary lymphoid structure. *Immunity.* 25:499–509.
37. Basak, S., H. Kim, J.D. Kearns, V. Tergaonkar, E. O'Dea, S.L. Werner, C.A. Benedict, C.F. Ware, G. Ghosh, I.M. Verma, and A. Hoffmann. 2007. A fourth IkappaB protein within the NF-kappaB signaling module. *Cell.* 128:369–381.
38. Weih, F., and J. Caamano. 2003. Regulation of secondary lymphoid organ development by the nuclear factor-kappaB signal transduction pathway. *Immunol. Rev.* 195:91–105.
39. Mackay, F., and J.L. Browning. 1998. Turning off follicular dendritic cells. *Nature.* 395:26–27.
40. Ware, C.F. 2005. Network communications: lymphotoxins, LIGHT, and TNF. *Annu. Rev. Immunol.* 23:787–819.
41. Lo, J.C., Y. Wang, A.V. Tumanov, M. Bamji, Z. Yao, C.A. Reardon, G.S. Getz, and Y.X. Fu. 2007. Lymphotoxin beta receptor-dependent control of lipid homeostasis. *Science.* 316:285–288.
42. Koch, A.E., G.K. Haines, R.J. Rizzo, J.A. Radosevich, R.M. Pope, P.G. Robinson, and W.H. Pearce. 1990. Human abdominal aortic aneurysms. Immunophenotypic analysis suggesting an immune-mediated response. *Am. J. Pathol.* 137:1199–1213.
43. Walton, L.J., J.T. Powell, and D.V. Parums. 1997. Unrestricted usage of immunoglobulin heavy chain genes in B cells infiltrating the wall of atherosclerotic abdominal aortic aneurysms. *Atherosclerosis.* 135:65–71.
44. Aubry, M.C., D.L. Riehle, W.D. Edwards, H. Maradit-Kremers, V.L. Roger, T.J. Sebo, and S.E. Gabriel. 2004. B-Lymphocytes in plaque and adventitia of coronary arteries in two patients with rheumatoid arthritis and coronary atherosclerosis: preliminary observations. *Cardiovasc. Pathol.* 13:233–236.
45. Tacke, F., D. Alvarez, T.J. Kaplan, C. Jakubzick, R. Spanbroek, J. Llodra, A. Garin, J. Liu, M. Mack, N. van Rooijen, et al. 2007. Monocyte subsets differentially employ CCR2, CCR5, and CX3CR1 to accumulate within atherosclerotic plaques. *J. Clin. Invest.* 117:185–194.
46. Zinkernagel, R.M., S. Ehl, P. Aichele, S. Oehen, T. Kundig, and H. Hengartner. 1997. Antigen localisation regulates immune responses in a dose- and time-dependent fashion: a geographical view of immune reactivity. *Immunol. Rev.* 156:199–209.
47. Mebius, R.E. 2003. Organogenesis of lymphoid tissues. *Nat. Rev. Immunol.* 3:292–303.
48. Gommerman, J.L., and J.L. Browning. 2003. Lymphotoxin/light, lymphoid microenvironments and autoimmune disease. *Nat. Rev. Immunol.* 3:642–655.
49. Moyron-Quiroz, J.E., J. Rangel-Moreno, K. Kusser, L. Hartson, F. Sprague, S. Goodrich, D.L. Woodland, F.E. Lund, and T.D. Randall. 2004. Role of inducible bronchus associated lymphoid tissue (iBALT) in respiratory immunity. *Nat. Med.* 10:927–934.
50. Browning, J.L. 2006. B cells move to centre stage: novel opportunities for autoimmune disease treatment. *Nat. Rev. Drug Discov.* 5:564–576.
51. Ludewig, B., S. Freigang, M. Jaggi, M.O. Kurrer, Y.-C. Pei, L. Vlk, B. Odermatt, R.M. Zinkernagel, and H. Hengartner. 2000. Linking immune-mediated arterial inflammation and cholesterol-induced atherosclerosis in a transgenic mouse model. *Proc. Natl. Acad. Sci. USA.* 97:12752–12757.
52. Timmer, T.C., B. Baltus, M. Vondenhoff, T.W. Huizinga, P.P. Tak, C.L. Verweij, R.E. Mebius, and T.C. van der Pouw Kraan. 2007. Inflammation and ectopic lymphoid structures in rheumatoid arthritis synovial tissues dissected by genomics technology: identification of the interleukin-7 signaling pathway in tissues with lymphoid neogenesis. *Arthritis Rheum.* 56:2492–2502.
53. Weyand, C.M., P.J. Kurtin, and J.J. Goronzy. 2001. Ectopic lymphoid organogenesis: a fast track for autoimmunity. *Am. J. Pathol.* 159: 787–793.
54. Lang, K.S., M. Recher, T. Junt, A.A. Navarini, N.L. Harris, S. Freigang, B. Odermatt, C. Conrad, L.M. Ittner, S. Bauer, et al. 2005. Toll-like receptor engagement converts T-cell autoreactivity into overt autoimmune disease. *Nat. Med.* 11:138–145.
55. Thaunat, O., A.C. Field, J. Dai, L. Louedec, N. Patey, M.F. Bloch, C. Mandet, M.F. Belair, P. Bruneval, O. Meilhac, et al. 2005. Lymphoid

neogenesis in chronic rejection: evidence for a local humoral alloimmune response. *Proc. Natl. Acad. Sci. USA*. 102:14723–14728.
56. Randolph, G.J., J. Ochando, and S. Partida-Sanchez. 2008. Migration of dendritic cell subsets and their precursors. *Annu. Rev. Immunol*. 26: 293–316.
57. Henderson, E.L., Y.J. Geng, G.K. Sukhova, A.D. Whittemore, J. Knox, and P. Libby. 1999. Death of smooth muscle cells and expression of mediators of apoptosis by T lymphocytes in human abdominal aortic aneurysms. *Circulation*. 99:96–104.
58. Ramshaw, A.L., and D.V. Parums. 1990. Immunohistochemical characterization of inflammatory cells associated with advanced atherosclerosis. *Histopathology*. 17:543–552.
59. Watanabe, M., A. Sangawa, Y. Sasaki, M. Yamashita, M. Tanaka-Shintani, M. Shintaku, and Y. Ishikawa. 2007. Distribution of inflammatory cells in adventitia changed with advancing atherosclerosis of human coronary artery. *J. Atheroscler. Thromb*. 14:325–331.
60. Schroder, A.E., A. Greiner, C. Seyfert, and C. Berek. 1996. Differentiation of B cells in the nonlymphoid tissue of the synovial membrane of patients with rheumatoid arthritis. *Proc. Natl. Acad. Sci. USA*. 93:221–225.
61. Shlomchik, M.J. 2008. Sites and stages of autoreactive B cell activation and regulation. *Immunity*. 28:18–28.
62. Swirski, F.K., P. Libby, E. Aikawa, P. Alcaide, F.W. Luscinskas, R. Weissleder, and M.J. Pittet. 2007. Ly-6Chi monocytes dominate hypercholesterolemia-associated monocytosis and give rise to macrophages in atheromata. *J. Clin. Invest*. 117:195–205.
63. Bettelli, E., M. Oukka, and V.K. Kuchroo. 2007. T(H)-17 cells in the circle of immunity and autoimmunity. *Nat. Immunol*. 8:345–350.
64. Olofsson, P.S., L.A. Soderstrom, D. Wagsater, Y. Sheikine, P. Ocaya, F. Lang, C. Rabu, L. Chen, M. Rudling, P. Aukrust, et al. 2008. CD137 is expressed in human atherosclerosis and promotes development of plaque inflammation in hypercholesterolemic mice. *Circulation*. 117:1292–1301.
65. Reardon, C.A., L. Blachowicz, T. White, V. Cabana, Y. Wang, J. Lukens, J. Bluestone, and G.S. Getz. 2001. Effect of immune deficiency on lipoproteins and atherosclerosis in male apolipoprotein E-deficient mice. *Arterioscler. Thromb. Vasc. Biol*. 21:1011–1016.
66. Rong, J.X., M. Shapiro, E. Trogan, and E.A. Fisher. 2003. Transdifferentiation of mouse aortic smooth muscle cells to a macrophage-like state after cholesterol loading. *Proc. Natl. Acad. Sci. USA*. 100:13531–13536.
67. Stopfer, P., D.N. Mannel, and T. Hehlgans. 2004. Lymphotoxin-beta receptor activation by activated T cells induces cytokine release from mouse bone marrow-derived mast cells. *J. Immunol*. 172:7459–7465.
68. Uzonyi, B., K. Lotzer, S. Jahn, C. Kramer, M. Hildner, E. Bretschneider, D. Radke, M. Beer, R. Vollandt, J.F. Evans, et al. 2006. Cysteinyl leukotriene 2 receptor and protease-activated receptor 1 activate strongly correlated early genes in human endothelial cells. *Proc. Natl. Acad. Sci. USA*. 103: 6326–6331.
69. Guthke, R., U. Moller, M. Hoffmann, F. Thies, and S. Topfer. 2005. Dynamic network reconstruction from gene expression data applied to immune response during bacterial infection. *Bioinformatics*. 21:1626–1634.
70. Bolstad, B.M., R.A. Irizarry, M. Astrand, and T.P. Speed. 2003. A comparison of normalization methods for high density oligonucleotide array data based on variance and bias. *Bioinformatics*. 19:185–193.
71. Benjamini, Y., and Y. Hochberg. 1995. Controlling the false discovery rate: A practical and powerful approach to multiple testing. *J. R. Stat. Soc. [Ser A]*. 57:289–300.
72. Bezdek, J.C. 1981. Pattern Recognition with Fuzzy Objective Function Algorithm. Plenum Press, New York.
73. Gentleman, R.C., V.J. Carey, D.M. Bates, B. Bolstad, M. Dettling, S. Dudoit, B. Ellis, L. Gautier, Y. Ge, J. Gentry, et al. 2004. Bioconductor: open software development for computational biology and bioinformatics. *Genome Biol*. 5:R80.
74. Kuhn, D.E., S. Roy, J. Radtke, S. Gupta, and C.K. Sen. 2006. Laser microdissection and pressure-catapulting technique to study gene expression in the reoxygenated myocardium. *Am. J. Physiol. Heart Circ. Physiol*. 290: H2625–H2632.
75. Sethi, N., and J. Palefsky. 2004. Transcriptional profiling of dysplastic lesions in K14-HPV16 transgenic mice using laser microdissection. *FASEB J*. 18:1243–1245.
76. Burgemeister, R., R. Gangnus, B. Haar, K. Schutze, and U. Sauer. 2003. High quality RNA retrieved from samples obtained by using LMPC (laser microdissection and pressure catapulting) technology. *Pathol. Res. Pract*. 199:431–436.
77. Wilhelm, D., R. Hiramatsu, H. Mizusaki, L. Widjaja, A.N. Combes, Y. Kanai, and P. Koopman. 2007. SOX9 regulates prostaglandin D synthase gene transcription in vivo to ensure testis development. *J. Biol. Chem*. 282: 10553–10560.